

DETC2005-85413

DESIGN OF PARALLEL KINEMATIC XY FLEXURE MECHANISMS

Shorya Awtar
Precision Engineering Research Group
Massachusetts Institute of Technology
77 Mass Ave 3-470, Cambridge, MA 02139
518-577-5500, shorya@mit.edu

Alexander H. Slocum
Department of Mechanical Engineering
Massachusetts Institute of Technology
77 Mass Ave 3-445, Cambridge, MA 02139
617-253-0012, slocum@mit.edu

ABSTRACT

This paper presents parallel kinematic XY mechanism designs that are based on a systematic constraint pattern. The constraint pattern, realized by means of double parallelogram flexure modules, is such that it allows large ranges of motion without over-constraining the mechanism or generating significant error motions. Nonlinear force-displacement characteristics of the double parallelogram flexure are used in analytically predicting the performance measures of the proposed XY mechanisms. Comparisons between closed-form linear and nonlinear analyses are presented to highlight the inadequacy of the former. Fundamental design tradeoffs in flexure mechanism performance are discussed qualitatively and quantitatively. It is shown that geometric symmetry in the constraint arrangement relaxes some of the design tradeoffs, resulting in improved performance. The nonlinear analytical predictions are validated by means of Finite Element Analysis and experimental measurements.

INTRODUCTION

Compact XY flexure stages that provide large range of motion are desirable in several applications such as semiconductor mask and wafer alignment [1], scanning interferometry and atomic force microscopy [2-3], micromanipulation and microassembly [4], high-density memory storage [5], and MEMS sensors and actuators [6-7]. Despite numerous designs that exist in the technical literature [1, 8-10], flexure stages generally lack adequate range of motion. Challenges in the design of large range mechanisms arise from the basic tradeoff between the quality of Degree of Freedom (DOF) and Degree of Constraint (DOC) in flexures [11]. As constraint elements, flexures pose a compromise between the primary motion along DOF and the stiffness and error motions along DOC. These tradeoffs are further

pronounced due to the nonlinear force-displacement characteristics that arise with increasing range of motion. Although deterministic mathematical techniques for flexure design exist and are very well suited for shape and size synthesis [12-13], principles of constraint design prove to be effective in topology generation [14]. Accordingly, based on a systematic and symmetric assembly of common flexure modules, several parallel kinematic XY mechanisms without over-constrained primary motions have been recently proposed [11, 15]. The underlying constraint arrangement in these designs, key performance measures and challenges, and some of the resulting mechanisms are presented in this paper.

A closed-form nonlinear analysis is employed to predict the performance of the proposed XY mechanisms, which utilize the simple-beam type double parallelogram flexure module. Non-linearities associated with beam curvature can be modeled using elliptical integrals [16] or pseudo-rigid body method [17], but are neglected since the beam deflections considered in the presented analysis are an order less than the beam length. However, the non-linearity arising from the force equilibrium expressions plays a significant role in determining the influence of loads and displacements in one direction on the stiffness properties of other directions, and therefore truly reveals the performance of the flexure mechanisms. This non-linearity can arise for displacements of the order of the beam thickness and has been thoroughly modeled in the prior literature using transcendental functions [18] and energy methods [19]. In this paper, we use simple yet accurate approximations [11, 20] for the pertinent non-linearity in the beam flexure and beam-based flexure modules. A realistic performance prediction, not possible using linear analysis, is thus obtained without the need for iterative or numerical methods. This closed-form analysis (CFA) offers a parametric understanding of the performance measures and tradeoffs therein, and provides a quantitative

validation of the design axiom that geometric symmetry yields improved flexure mechanism performance.

XY MECHANISM TOPOLOGY DESIGN

There are two kinds of design configurations for multi DOF mechanisms – serial and parallel. Serial designs present a stacked assembly of several single-DOF stages and incorporate moving actuators and cables, which can be detrimental for precision and dynamic performance. Parallel designs, which are considered here, are usually compact and allow ground mounting of actuators. The important performance measures of a parallel kinematic XY flexure mechanism and associated challenges are listed here.

1. The primary objective of the design is to achieve large ranges of motion along the desired directions X and Y, and an obvious limitation comes from material failure criteria. For a given maximum stress level, high compliance in the directions of primary motion or DOF increases the range of motion. However, for non-planer designs, this conflicts with the need to maintain high stiffness and small error motions in the out-of-plane directions.

2. In an XY mechanism, the motion stage yaw is often undesirable. Given this requirement, the motion stage yaw may be rejected passively or actively. While both options have respective advantages, fewer actuators make the former preferable due to reduced design complexity and potentially better motion range. Thus, the mechanism has to be designed such that the rotation of the motion stage, being a *parasitic error*, is inherently constrained. Furthermore, determination of the *Center of Stiffness* of the motion stage in the mechanism with respect to actuation forces is of key importance.

3. Minimal *cross-axis coupling* between the X and Y degrees of freedom is an important performance requirement, especially in applications where end-point feedback is not feasible or the two axes are not actively controlled. In the absence of end-point feedback, an additional calibration step is necessary to determine the transformation matrix between the actuator coordinates and the motion stage coordinates. In unactuated or under-actuated systems, cross-axis coupling can lead to undesirable internal resonances.

4. An important challenge in parallel mechanism design for positioning is that of integrating the ground-mounted actuators with the motion stage. Displacement source actuators, which are preferable due to their high force capacity, do not tolerate transverse loads and displacements. Therefore, the point of actuation on the flexure mechanism must be such that it only moves along the direction of actuation and has minimal transverse motions in response to any actuator in the system. Eliminating transverse motion at the point of actuation, is termed as *actuator isolation*, and is generally difficult to achieve due to the parallel geometry.

5. In the absence of adequate actuator isolation, the actuators have to be connected to the point of actuation by means of a decoupler, which ideally transmits axial force without any loss in motion and absorbs any transverse motions without

generating transverse loads. However, a flexure-based decoupler, which is desirable to maintain precision, is subject to its own tradeoffs. Increasing its motion range and compliance in the transverse direction results in an error motion along its axial direction, and a loss in *inline stiffness*. The inline stiffness is the overall stiffness between the point of actuation and the motion stage, and influences the dynamic performance of the motion system.

6. Low thermal and manufacturing sensitivity are important performance parameters for precision mechanisms in general. Both these factors, being strongly dependent on the mechanism's geometry, may be improved with the careful use of reversal and symmetry.

Because of the tradeoff between quality of DOF and DOC, all these performance measures including parasitic errors, cross-axis coupling, actuator isolation, lost motion and inline stiffness, deteriorate with increasing range of motion. Depending upon the application, these collectively restrict the range of a parallel kinematic mechanism to a much smaller level than what is allowed by material limits. While geometric symmetry plays an important role in improving performance, if implemented inappropriately, it can overconstrain the primary motions resulting in a significantly reduced range.

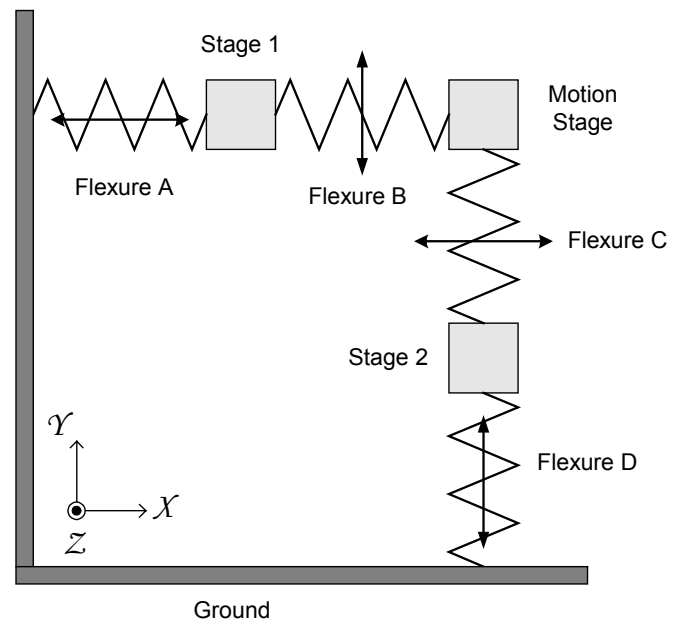


Fig.1 Proposed Constraint Arrangement for XY Flexure Mechanisms

Fig. 1 illustrates the proposed constraint arrangement that can help achieve the above-listed desirable attributes in XY mechanisms. The constraint arrangement includes four basic rigid stages: Ground, Motion Stage, and intermediate stages 1 and 2. Stage 1 is connected to Ground by means of flexure A, which only allows relative X translation; the Motion Stage is connected to Stage 1 via flexure B, which only allows relative Y translation; the Motion Stage is connected to Stage 2 via flexure C, which only allows a relative X translation; and

finally, Stage 2 is connected to Ground by means of flexure D, which only allows relative Y translation. Thus, in any deformed configuration of the mechanism, Stage 1 will always have only an X displacement with respect to Ground while Stage 2 will have only a Y displacement. Furthermore, the Motion Stage inherits the X displacement of Stage 1 and the Y displacement of Stage 2, thus acquiring two translational degrees of freedom that are mutually independent. Since the Y and X displacements of the Motion Stage do not influence Stage 1 and Stage 2, respectively, these intermediate stages are ideal actuator locations that obviate the need for decouplers.

In an ideal scenario where flexures A, B, C and D are perfect constraints, this arrangement would yield a flawless design. However, due to the inherent imperfection in flexures, the actual resulting designs are expected to deviate slightly from ideal behavior. Any approximately linear motion flexure unit can be used as the building block flexures A, B, C and D. Fig.2 presents a design based on the simple-beam type double parallelogram flexure. Reasons for this choice include large range, good rotational stiffness, no purely kinematic parasitic errors, and excellent thermal stability. Without causing overconstraint, this design is further enhanced by making insightful use of symmetry, which involves adding intermediate stages 3 and 4, and repeating the constraint arrangement described earlier. The resulting design, illustrated in Fig. 7, is expected to exhibit superior performance. Since the relative rotation in the double parallelogram module is elastic and elastokinematic in nature [11, 20], motion stage rotation in both these mechanisms may be mitigated by appropriately locating the actuation forces on the intermediate stages. The axes of X and Y actuation that minimize the motion stage yaw are referred to as the *Center of Stiffness (COS)* axes.

Several other XY designs with different space utilization, choice of building blocks, and levels of symmetry can be generated using the proposed constraint arrangement [15]. The performance of any resulting mechanism depends on the choice of building blocks and the geometry of the constraint arrangement, as shall be shown analytically in the following sections.

PARALLELOGRAM FLEXURE AND VARIATIONS

The non-dimensionalized force-displacement relationships for the double parallelogram flexure and the relevant nomenclature are provided in the Appendix. All displacements and length parameters are normalized by the beam length L , forces by $E'I_{zz}/L^2$, and moments by $E'I_{zz}/L$. E' denotes Young's modulus for plane stress, and plate modulus for plane strain. Non-dimensional quantities are represented by lower case letters throughout this paper. The secondary stage of the double parallelogram flexure and all the moving stages in the proposed designs are assumed rigid. In analyzing the mechanism designs, force equilibrium is applied in the deformed configuration of the mechanism to capture the relevant non-linearities. Stage rotations, being small, are neglected wherever their contribution is relatively insignificant.

XY Mechanism Design 1

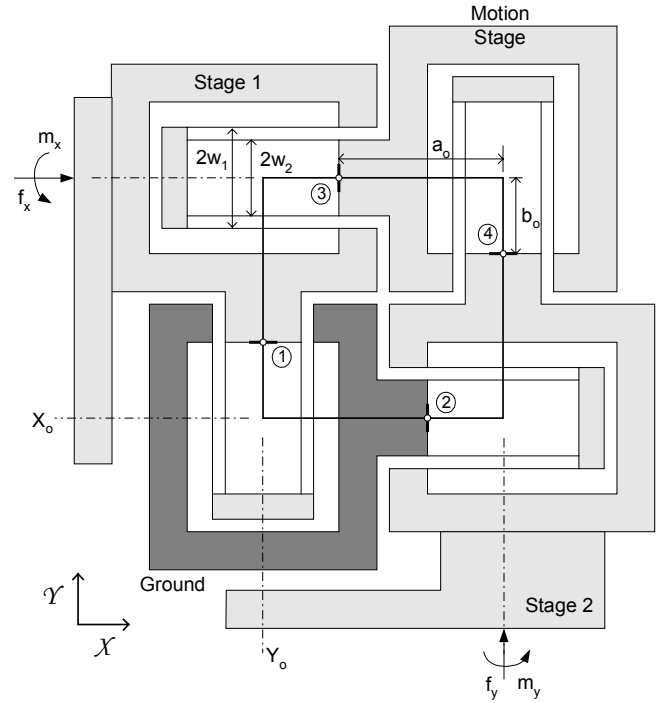


Fig.2 XY Mechanism Design 1

XY Mechanism Design 1 is shown in a deformed configuration in Fig. 3, where the rigid frames including ground, motion stage and the two intermediate stages are represented by solid lines, and the compliance of the double parallelograms is represented by the small circles. The relative displacements of each constituent flexure module are given by,

λ	θ_λ	y_λ	x_λ
1	θ_1	$x_1 + a_0\theta_1$	y_1
2	θ_2	$y_2 - b_0\theta_2$	x_2
3	$\theta_s - \theta_1$	$(y_s - a_0\theta_s) - (y_1 + b_0\theta_1)$	$x_s - x_1$
4	$\theta_s + \theta_2$	$(x_2 - a_0\theta_2) - (x_s + b_0\theta_s)$	$y_s - y_2$

There are three internal forces per flexure module and three displacements per stage, resulting in 21 unknowns. The three force-displacement relations per flexure module and three force-equilibrium relations per stage provide 21 equations. Since the internal forces are not of interest, instead of solving these equations explicitly, energy methods are employed to efficiently obtain the following summarized force-displacement results for the linear case.

$$\begin{Bmatrix} f_x \\ f_y \\ m_x \\ m_y \\ 0 \end{Bmatrix} = \begin{bmatrix} k_1 & 0 & -k_2 & -k_2 & -k_3 \\ 0 & k_1 & k_3 & k_3 & k_2 \\ -k_2 & k_3 & k_4 & 0 & -k_5 \\ -k_2 & k_3 & 0 & k_4 & -k_5 \\ -k_3 & k_2 & -k_5 & -k_5 & k_4 \end{bmatrix} \begin{Bmatrix} x_s \\ y_s \\ \theta_1 \\ \theta_2 \\ \theta \end{Bmatrix} \quad (1)$$

$$k_1 = 2a$$

$$k_2 = -a(a_o + \frac{1}{2})$$

where, $k_3 = -a(b_o - \frac{1}{2})$

$$k_4 = a(a_o^2 + b_o^2) - a(b_o - a_o) + 2\bar{w}^2 d$$

$$k_5 = \frac{1}{2}a(b_o - a_o) - a(a_o b_o)$$

The motion stage rotation can be obtained by inverting the above stiffness matrix.

$$\theta_s = \frac{1}{k_4} (m_x - f_x(a_o + b_o) + m_y + f_y(a_o + b_o))$$

This expression shows that the motion stage rotation can be made identically zero if $m_x = f_x(a_o + b_o)$ and $m_y = -f_y(a_o + b_o)$, which implies that the COS axes for the motion stage with respect to the X and Y actuation forces is given by X_o and Y_o , shown in Fig. 2. Not being intuitively obvious, this is an important finding if motion stage yaw is to be minimized passively. With this choice of actuation force location, the remaining displacements may be calculated from (1).

$$\begin{aligned} x_s &= \frac{f_x}{2a} + \frac{(2a_o + 1)^2}{16\bar{w}^2 d} f_y; & x_1 &= x_s + \frac{f_x}{2d}; & x_2 &= \frac{f_x}{2d} \\ y_s &= \frac{f_y}{2a} + \frac{(2b_o - 1)^2}{16\bar{w}^2 d} f_x; & y_1 &= \frac{f_y}{2d}; & y_2 &= y_s + \frac{f_y}{2d} \\ \theta_1 &= -\frac{(1 - 2a_o - 4b_o)}{8\bar{w}^2 d} f_x - \frac{(1 - 2b_o)}{8\bar{w}^2 d} f_y \\ \theta_2 &= -\frac{(1 + 2a_o)}{8\bar{w}^2 d} f_x - \frac{(1 + 4a_o + 2b_o)}{8\bar{w}^2 d} f_y \end{aligned} \quad (2)$$

Since the linear analysis captures only elastic effects, it should be recognized that these results are valid only for small loads and displacements. Nevertheless, they provide valuable design help not only in determining the actuator locations but also in selecting the geometric parameters a_o and b_o so as to minimize cross-axis coupling and intermediate stage rotations. In this case, dimension a_o should be kept as small as possible and b_o should be chosen to be $1/2$.

To accurately predict the elastokinematic effects that become prominent with increasing loads and displacements, we proceed to perform a non-linear analysis. The 21 equations, including the non-linear force displacement relations for the double parallelogram listed in the Appendix, are explicitly solved using the symbolic computation tool MAPLE™. Taking advantage of the normalized framework, insignificant terms are dropped at appropriate steps in the analysis, and the following force-displacement results for the mechanism are obtained.

$$x_s = \frac{\left[8af_x + \frac{a^2(1+2a_o)}{\bar{w}^2 d} f_y - 8a^2(a_o\theta_1 + a_o\theta_2 + b_o\theta_s) \right]}{(4a)^2 - (ef_y)^2} \quad (3)$$

$$y_s = \frac{\left[8af_y + \frac{a^2(1-2b_o)}{\bar{w}^2 d} f_x + 8a^2(b_o\theta_1 + b_o\theta_2 + a_o\theta_s) \right]}{(4a)^2 - (ef_x)^2} \quad (4)$$

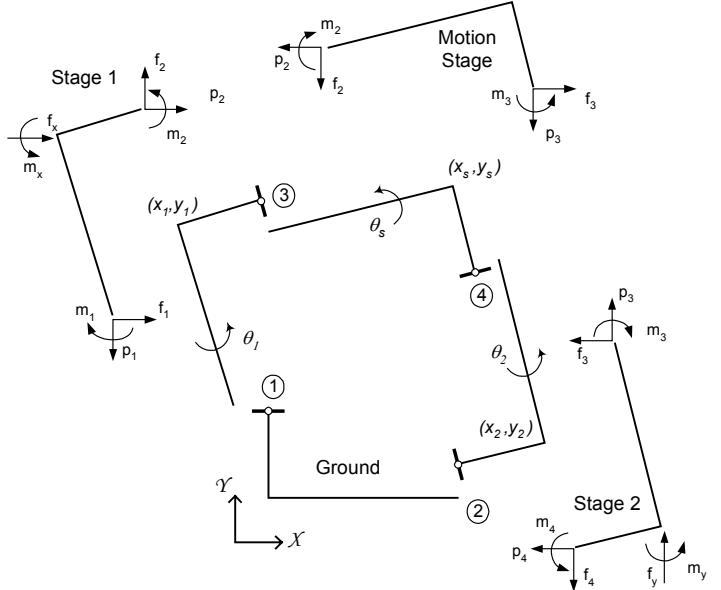


Fig.3 XY Mechanism 1 in a Deformed Configuration

$$x_1 = x_s + \left[\frac{y_2^2(ra/2 - ei)}{4a} + \frac{1}{2d} \right] f_x \quad (5)$$

$$y_1 = \left[\frac{x_1^2(ra/2 - ei)}{4a} + \frac{1}{2d} \right] f_y$$

$$y_2 = y_s + \left[\frac{x_1^2(ra/2 - ei)}{4a} + \frac{1}{2d} \right] f_y \quad (6)$$

$$x_2 = \left[\frac{y_2^2(ra/2 - ei)}{4a} + \frac{1}{2d} \right] f_x$$

While the results of the linear and non-linear analyses match exactly for small loads and displacements, it is apparent that the latter is necessary to predict several factors that contribute to the mechanism's performance attributes. Expressions (3) and (4) indicate that the primary motion stiffness drops as a quadratic function of the actuation force in the other direction. Over a typical force range of ± 2.4 required to produce ± 0.1 displacements, the primary stiffness variation is less than 0.4%. Furthermore, the cross-axis coupling has both a linear as well as a quadratic component. While the linear component along y_s in response to f_x may be eliminated by the choice of $b_o = 1/2$, no such remedy is available for the other direction. This is clearly a consequence of the lack of symmetry between the X and Y axes in this design.

Expressions (5) and (6) predict the degree of actuator isolation, lost motion, and inline stiffness. For a given motion stage X displacement, Stage 1 experiences both an X displacement as well as a Y displacement in response to a Y actuation force. The former is a consequence of the elastokinematic effects in flexure module 2, while the latter results due to the elastokinematic effect in flexure module 1. The axial compliance of flexure module 2 contributes to the

overall inline compliance between the X actuator and the motion stage, and is given by

$$\frac{\partial(x_l - x_s)}{\partial f_x} = \frac{l}{2d} + \frac{y_2^2}{4} \left(\frac{r}{2} - \frac{ei}{a} \right) \quad (7)$$

Lost motion and loss of inline stiffness, predicted above, are plotted in Fig. 4, along with FEA results for a given geometry ($a_o=0.9737$, $b_o=0.5$, $t=1/76$, $L=60mm$). Although not significant for small displacements, the predicted drop in axial stiffness is approximately 90% from the nominal value, for displacements of the order of ± 0.1 and is of concern for both static and dynamic performance.

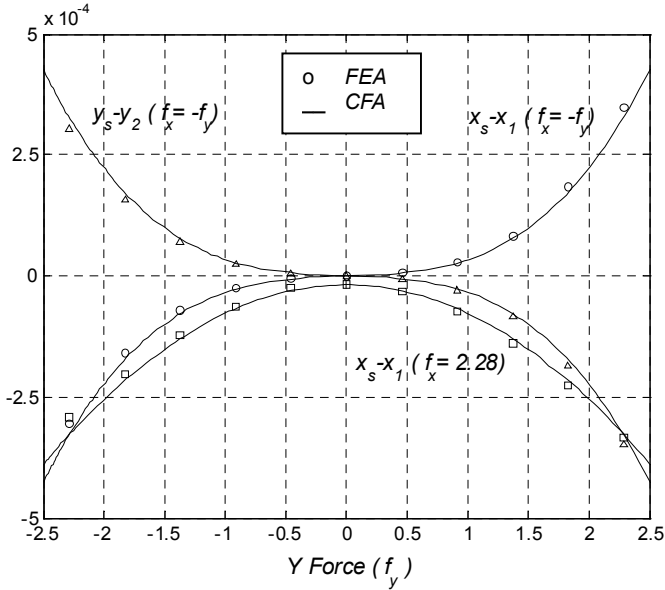


Fig.4 Lost Motion and Inline Stiffness

For simplicity, motion stage rotation is expressed here for two special cases.

For $f_y = 0 = m_y$,

$$\theta_s = \frac{[32a^2(m_x - a_o f_x - b_o f_x) + rd(2m_x - a_o f_x - b_o f_x)f_x^2]}{64a^2 \bar{w}^2 d} \quad (8)$$

For $f_x = 0 = m_x$,

$$\theta_s = \frac{[32a^2(m_y + a_o f_y + b_o f_y) + rd(2m_y + a_o f_y + b_o f_y)f_y^2]}{64a^2 \bar{w}^2 d}$$

For small loads and displacements, these expressions yield COS identical to those predicted by the linear analysis. With no independent moments, and actuation forces acting along axes X_o and Y_o the above expressions reduce to

$$\text{For } f_y = 0 = m_y, \quad \theta_s = \frac{r(a_o + b_o)}{64a^2 \bar{w}^2} f_x^3 \quad (9)$$

$$\text{For } f_x = 0 = m_x, \quad \theta_s = -\frac{r(a_o + b_o)}{64a^2 \bar{w}^2} f_y^3$$

This shows that while it is possible to eliminate the linear, or purely elastic, component of the motion stage rotation by selecting the force locations, the same is not true for the non-linear elastokinematic components because the COS shifts with increasing loads. Since the applied moments cannot be controlled independent of the forces, the mechanism's geometry plays an important role in the effectiveness of this passive yaw minimization method. Motion stage rotation is plotted against the X and Y actuation forces in Fig. 5. This not only illustrates the inadequacy of the linear analysis, but also gives an idea of the range beyond which the non-linear effects become important. For the given dimensions mentioned earlier, the maximum rotation is approximately $40 \mu\text{rad}$ over a motion range of ± 0.1 . However, to ensure a motion stage rotation of less than $5 \mu\text{rad}$, the motion range of this mechanism is restricted to 0.05 .

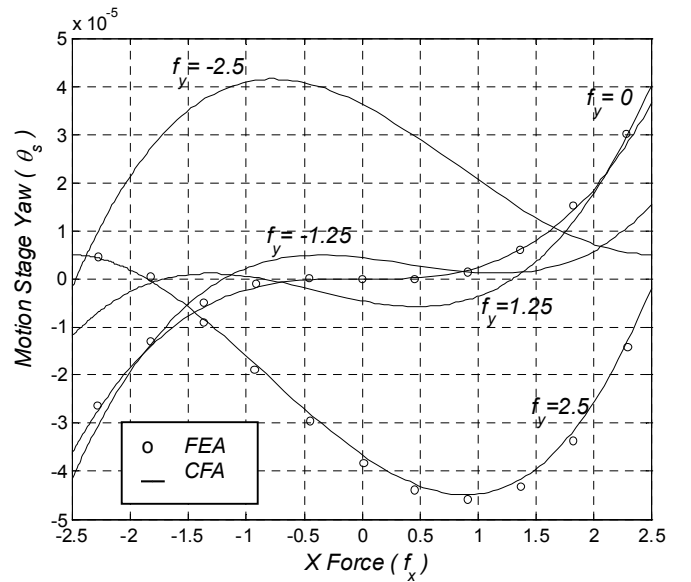
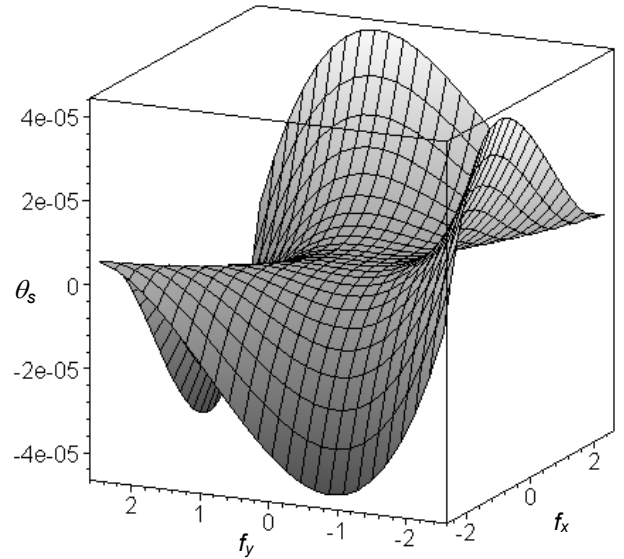


Fig. 5 Motion Stage Rotation

Sensitivity of the motion stage yaw to the location of force application may also be analytically determined to simulate assembly and manufacturing tolerances that can cause a misalignment between the COS axis and the actuator axis. If e_x is the offset between the desirable axis X_o and the actual actuation axis, then the motion stage yaw is given by the following expression in the absence of any Y actuation force.

$$\theta_s = \frac{l}{64a^2\bar{w}^2} \left[r(a_o + b_o + 2e_x)f_x^3 + \frac{32a^2e_x}{d}f_x \right] \quad (10)$$

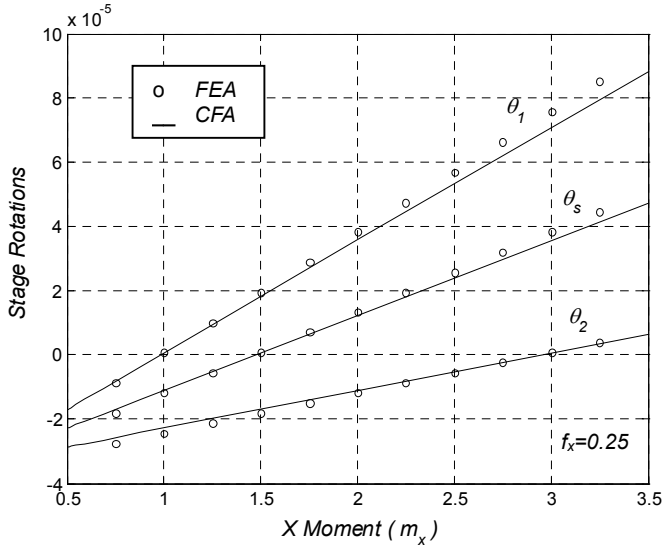


Fig.6 Center of Stiffness of the Stages with respect to X Force

This prediction is corroborated by FEA in Fig. 6. If the application so demands, the actuation forces may be alternatively applied along the COS axes of Stage 1 or Stage 2, but this obviously affects the motion stage rotation. Using the linear and non-linear analyses, it is found that the COS for Stage 1 with respect to X actuation force is located at a distance $(1+2b_o+4a_o)/6$ from the nominal location, and with respect to the Y actuation force is located at $(1-2a_o-4b_o)/2$, which actually corresponds to the Y_o axis for $b_o=0.5$. Similarly, the COS of Stage 2 with respect to the Y actuation force is located at a distance $(1-2a_o-4b_o)/6$ from the nominal location, and with respect to X actuation force is located at $(1+2b_o+4a_o)/2$. A force location that results in positive moment, following the convention of Fig. 2, is considered positive and vice versa. These results are precisely validated in Fig. 6.

With actuation forces applied along the COS of the motion stage, the intermediate stage rotations are calculated from the non-linear analysis for specific cases.

$$\text{For } f_x = 0, \theta_1 = \frac{16a^2(2b_o - 1)f_y - rd(a_o - b_o + 1)f_y^3}{4\bar{w}^2d(rd f_y^2 + 32a^2)} \quad (11)$$

$$\theta_2 = \frac{rd f_y^2 + 16a^2}{rd f_y^2 + 32a^2} \frac{[-16a^2(1+2b_o+4a_o)f_y - rd(a_o+b_o)f_y^3]}{64a^2\bar{w}^2d}$$

$$\text{For } f_y = 0, \theta_2 = \frac{[-16a^2(1+2a_o)f_x - rd(a_o - b_o + 1)f_x^3]}{4\bar{w}^2d(rd f_x^2 + 32a^2)} \quad (12)$$

$$\theta_1 = \frac{rd f_x^2 + 16a^2}{rd f_x^2 + 32a^2} \frac{[-16a^2(1-2a_o-4b_o)f_x + rd(a_o+b_o)f_x^3]}{64a^2\bar{w}^2d}$$

The intermediate stage rotations are obviously large and have a dominant linear component, with the non-linear contribution two orders of magnitude smaller. The dependence of Stage 1 rotation on f_y is clearly attenuated with the choice of $b_o=1/2$ as discussed above. This is not true of Stage 2, which therefore sees a higher maximum rotation. This difference between the behaviors of the two intermediate stages is due to the lack of symmetry between the two.

XY Mechanism Design 2

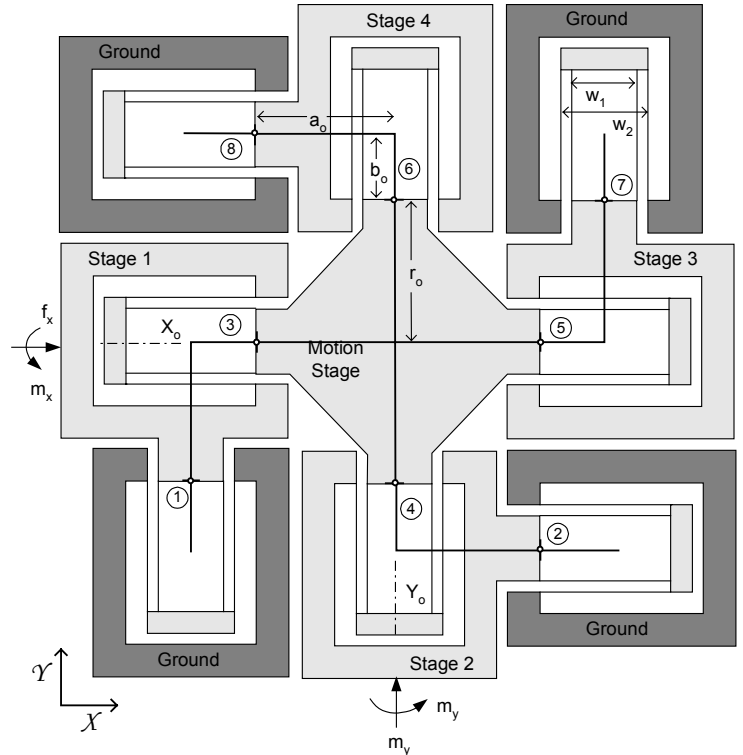


Fig.7 XY Mechanism Design 2

Fig.8 illustrates the XY Mechanism Design 2 in a deformed configuration, along with the FBD and displacements of the stages. The relative displacements for each of the double parallelogram flexure modules, represented by the small circles, are given by

λ	θ_λ	y_λ	x_λ
1	θ_1	$x_1 - a_o\theta_1$	y_1
2	θ_2	$y_2 + a_o\theta_2$	$-x_2$
3	$\theta_s + \theta_1$	$(y_s - r_o\theta_s) - (y_1 - b_o\theta_1)$	$x_s - x_1$

4	$\theta_s + \theta_2$	$-(x_s + r_o \theta_s) + (x_2 + b_o \theta_2)$	$y_s - y_2$
5	$\theta_s - \theta_7$	$-(y_s + r_o \theta_s) + (y_7 - b_o \theta_7)$	$-x_s + x_7$
6	$\theta_s - \theta_8$	$(x_s - r_o \theta_s) - (x_8 + b_o \theta_8)$	$-y_s + y_8$
7	θ_7	$x_7 - a_o \theta_7$	$-y_7$
8	θ_8	$y_8 - a_o \theta_8$	x_8

There are 3 unknown displacements per stage and 3 unknown internal forces per flexure module, resulting in 39 unknowns. The 3 force equilibrium relations per stage and 3 constitutive relations per flexure module provide 39 equations necessary to solve these unknowns. Once again, a linear analysis is performed first, using linear constitutive relations for the modules, and yields the following force-displacement results for the overall mechanism.

$$\begin{bmatrix} k_1 & 0 & k_2 & k_3 & k_2 & k_3 & 0 \\ 0 & k_1 & -k_3 & k_2 & -k_3 & k_2 & 0 \\ k_2 & -k_3 & k_4 & 0 & 0 & 0 & -k_5 \\ k_3 & k_2 & 0 & k_4 & 0 & 0 & -k_5 \\ k_2 & -k_3 & 0 & 0 & k_4 & 0 & k_5 \\ k_3 & k_2 & 0 & 0 & 0 & k_4 & k_5 \\ 0 & 0 & -k_5 & -k_5 & k_5 & k_5 & k_6 \end{bmatrix} \begin{bmatrix} x_s \\ y_s \\ \theta_1 \\ \theta_2 \\ \theta_7 \\ \theta_8 \\ \theta_s \end{bmatrix} = \begin{bmatrix} f_x \\ f_y \\ -m_x \\ -m_y \\ 0 \\ 0 \\ 0 \end{bmatrix} \quad (13)$$

$$k_1 = 4a; \quad k_2 = -a(a_o + \frac{1}{2}); \quad k_3 = -a(b_o - \frac{1}{2})$$

$$k_4 = a(a_o^2 + b_o^2) - a(b_o - a_o) + 2\bar{w}^2 d$$

where,

$$k_5 = ab_o(r_o + \frac{1}{2}) + (\frac{1}{2}ar_o + \bar{w}^2 d)$$

$$k_6 = 4ar_o(r_o + \frac{1}{2}) + 4(\frac{1}{2}ar_o + \bar{w}^2 d)$$

These equations may be further solved determine the displacements explicitly.

$$x_s = \frac{f_x}{4a} - \frac{(2a_o + 1)m_x}{16d\bar{w}^2} - \frac{(2b_o - 1)m_y}{16d\bar{w}^2}$$

$$x_1 = x_s + \frac{3f_x}{4d}; \quad x_2 = \frac{f_x}{4d}; \quad x_7 = x_s - \frac{f_x}{4d}; \quad x_8 = \frac{f_x}{4d}$$

$$y_s = \frac{f_y}{4a} + \frac{(2b_o - 1)m_x}{16d\bar{w}^2} - \frac{(2a_o + 1)m_y}{16d\bar{w}^2}$$

$$y_1 = \frac{f_y}{4d}; \quad y_2 = y_s + \frac{3f_y}{4d}; \quad y_7 = \frac{f_y}{4d}; \quad y_8 = y_s - \frac{f_y}{4d}$$

$$\theta_1 = \frac{(2a_o + 1)f_x}{16d\bar{w}^2} - \frac{(2b_o - 1)f_y}{16d\bar{w}^2} - \frac{5m_x}{8d\bar{w}^2} - \frac{m_y}{8d\bar{w}^2}$$

$$\theta_2 = \frac{(2a_o + 1)f_y}{16d\bar{w}^2} + \frac{(2b_o - 1)f_x}{16d\bar{w}^2} - \frac{m_x}{8d\bar{w}^2} - \frac{5m_y}{8d\bar{w}^2}$$

$$\theta_7 = \frac{(2a_o + 1)f_x}{16d\bar{w}^2} - \frac{(2b_o - 1)f_y}{16d\bar{w}^2} + \frac{m_x}{8d\bar{w}^2} + \frac{m_y}{8d\bar{w}^2}$$

$$\theta_8 = \frac{(2a_o + 1)f_y}{16d\bar{w}^2} + \frac{(2b_o - 1)f_x}{16d\bar{w}^2} + \frac{m_x}{8d\bar{w}^2} + \frac{m_y}{8d\bar{w}^2}$$

$$\theta_s = \frac{m_x}{4d\bar{w}^2} + \frac{m_y}{4d\bar{w}^2} \quad (14)$$

Several interesting observations can be made from this preliminary analysis. Motion stage rotation is predicted to be identically zero, irrespective of dimensions, in the absence of any applied moments. This implies that the COS axes of the motion stage correspond to X_o and Y_o , shown in Fig. 8. Furthermore the elastic contribution in the error motions can be minimized by choosing the smallest possible a_o , and $b_o=1/2$. With this choice of design parameters, the above results also show that the rotations of intermediate stages 1 and 3 are not be affected by the Y actuation force, and those of intermediate stages 2 and 4 are not affected by X actuation forces.

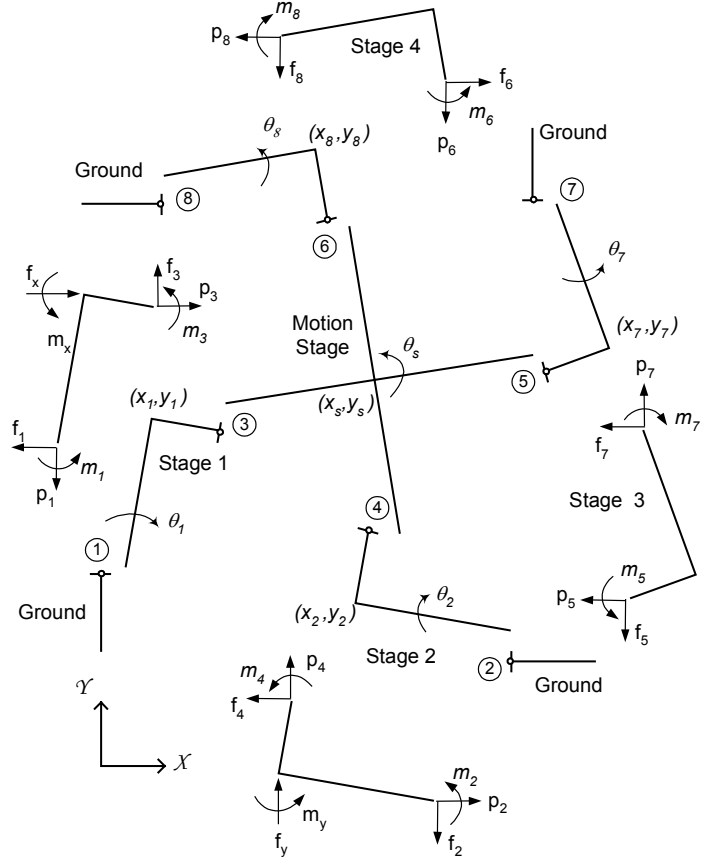


Fig.8 XY Mechanism 2 in a Deformed Configuration

A more accurate prediction of the mechanism behavior is obtained by solving the system equations using the nonlinear force-displacement relations for the modules. By neglecting insignificant terms at each step in the derivation, the following displacement results are obtained using MAPLE™.

$$x_s = \frac{f_x (64a^2 + y_2^2 e^3 f_y^2)}{4a (64a^2 - 3e^2 f_y^2)} \approx \frac{f_x}{4a} \frac{64a^2}{(64a^2 - 3e^2 f_y^2)} \quad (15)$$

$$y_s = \frac{f_y (64a^2 + x_1^2 e^3 f_x^2)}{4a (64a^2 - 3e^2 f_x^2)} \approx \frac{f_y}{4a} \frac{64a^2}{(64a^2 - 3e^2 f_x^2)} \quad (16)$$

$$x_1 = \frac{f_x}{4a} \frac{64a^2}{(64a^2 - 3e^2 f_y^2)} - \frac{f_x y_2^2 ei (192a^2 - 11e^2 f_y^2)}{8a (64a^2 - 3e^2 f_y^2)} \quad (17)$$

$$\approx \frac{f_x}{4a} \frac{64a^2}{(64a^2 - 3e^2 f_y^2)} + \frac{3f_x}{4} \left(-\frac{y_2^2 ei}{2a} + \frac{1}{d} \right)$$

$$x_7 = \frac{f_x}{4a} \frac{64a^2}{(64a^2 - 3e^2 f_y^2)} + \frac{f_x y_2^2 ei (64a^2 - e^2 f_y^2)}{8a (64a^2 - 3e^2 f_y^2)} \quad (18)$$

$$\approx \frac{f_x}{4a} \frac{64a^2}{(64a^2 - 3e^2 f_y^2)} - \frac{f_x}{4} \left(-\frac{y_2^2 ei}{2a} + \frac{1}{d} \right)$$

$$x_2 = \frac{f_x}{4} \left(-\frac{y_2^2 ei}{2a} + \frac{1}{d} \right); \quad x_8 = \frac{f_x}{4} \left(-\frac{y_2^2 ei}{2a} + \frac{1}{d} \right) \quad (19)$$

$$y_2 = \frac{f_y}{4a} \frac{64a^2}{(64a^2 - 3e^2 f_x^2)} - \frac{f_y x_1^2 ei (192a^2 - 11e^2 f_x^2)}{8a (64a^2 - 3e^2 f_x^2)} \quad (20)$$

$$\approx \frac{f_y}{4a} \frac{64a^2}{(64a^2 - 3e^2 f_x^2)} + \frac{3f_y}{4} \left(-\frac{x_1^2 ei}{2a} + \frac{1}{d} \right)$$

$$y_8 = \frac{f_y}{4a} \frac{64a^2}{(64a^2 - 3e^2 f_x^2)} + \frac{f_y x_1^2 ei (64a^2 - e^2 f_x^2)}{8a (64a^2 - 3e^2 f_x^2)} \quad (21)$$

$$\approx \frac{f_y}{4a} \frac{64a^2}{(64a^2 - 3e^2 f_x^2)} - \frac{f_y}{4} \left(-\frac{x_1^2 ei}{2a} + \frac{1}{d} \right)$$

$$y_1 = \frac{f_y}{4} \left(-\frac{x_1^2 ei}{2a} + \frac{1}{d} \right); \quad y_7 = \frac{f_y}{4} \left(-\frac{x_1^2 ei}{2a} + \frac{1}{d} \right) \quad (22)$$

As in the previous case, the non-linear analysis captures several factors that determine the mechanism's performance but are not predicted by the linear analysis. Since this design has twice as many flexure modules, the force required to generate a nominal primary motion of ± 0.1 , approximately 4.8, is also twice that for Design 1. It may be noticed in (15) that the stiffness in the primary direction X changes with the application of a Y force. This is expected because with the application of a positive Y force, flexure modules 4, 6 and 7 experience a compressive axial force, while module 1 sees a tensile axial force. Irrespective of whether the axial force is tensile or compressive, the transverse stiffness of all these units drops resulting in an overall all reduction in the primary motion stiffness. Over the range of applied force, the drop in primary stiffness is less than 1.2%.

Expressions (15) and (16) show that the linear elastic component of the cross-axis coupling in this case is entirely eliminated. Any contributions from the applied moments and stage rotations are effectively cancelled out due symmetry. However, there remains a quadratic elastokinematic component comparable to that in Design 1, and is plotted in Fig. 9 for geometric dimensions analogous to Design 1 ($a_o=0.9737$, $b_o=0.5$, $r_o=0.9737$, $t=1/76$, $L=60mm$). Intermediate stage 1 experiences an additional X displacement arising from the nonlinear elastokinematic effect of flexure unit 3, in the

presence of an X actuation force and Y primary motion. It also exhibits a Y displacement resulting from the elastokinematic effect of flexure unit 1, in the presence of a Y actuation force and X primary motion. Thus, actuator isolation in terms of transverse displacements x_2 and y_1 remains comparable to the previous design, however intermediate stage rotations are reduced, as shown later.

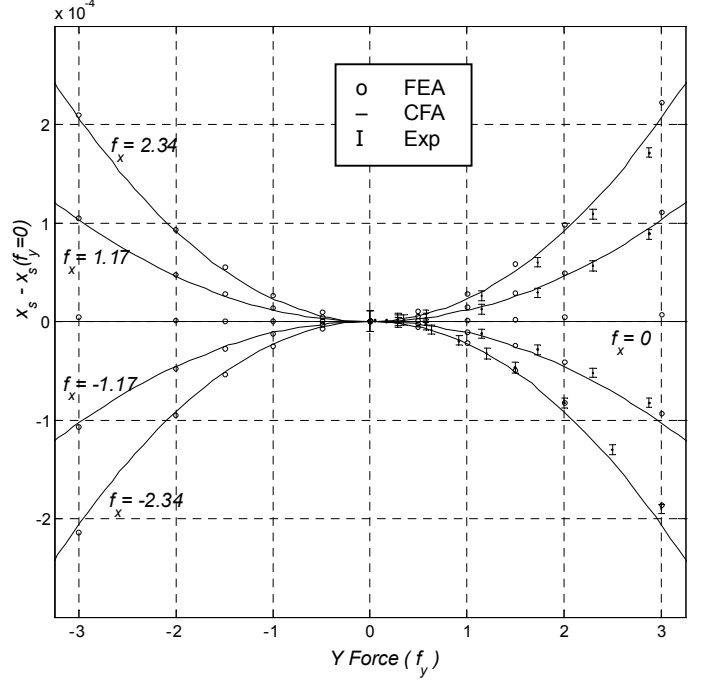


Fig. 9 Cross-axis Errors in X Direction

Lost motion and change in inline stiffness is given by expressions (17) and (20). The higher order elastokinematic terms may be neglected because they are about two orders smaller than the next larger terms. As in the previous case, the inline stiffness between the actuator and motion reduces with increasing primary motions, owing to the double parallelogram characteristics. Stiffness between the point of actuation and motion stage is easily obtained from (17), and is similar in nature and magnitude to the previous design. Both these performance attribute predictions are validated in Fig. 10 by means of FEA and experimental measurements.

The stage rotations can also be analytically calculated and the nonlinear results are presented here for some specific cases. Motion stage rotation is given by

$$\text{For } f_y = 0 = m_y, \quad \theta_s = \frac{(64a^2 + rdf_x^2)}{256a^2 \bar{w}^2 d} m_x \quad (23)$$

$$\text{For } f_x = 0 = m_x, \quad \theta_s = \frac{(64a^2 + rdf_y^2)}{256a^2 \bar{w}^2 d} m_y$$

This validates the inference drawn from the linear analysis regarding the COS location. Remarkably, this choice of COS axes which corresponds $m_x = m_y = 0$ not only eliminates the linear elastic component in the motion stage rotation, but also the non-linear terms. The overall dependence of motion stage rotation

on the actuation forces X and Y is presented in Fig. 11. It is apparent from the large flat area in the central region of this plot, that motion stage rotation has been considerably suppressed despite the elastokinematic errors of the double parallelogram flexure module. In fact, it is possible to keep the motion stage rotation less than $5 \mu\text{rad}$ over a motion range of $+0.1/-0.05$. Experimental measurements of the stage rotation presented in Fig.12, show a random variation within $\pm 2 \mu\text{rad}$, which is very likely due to environmental drift. Expressions (23) also provide a quantitative assessment of the sensitivity of the stage rotation with respect to an offset in the actuation axis. This is two times better than the previous design for small loads, and four times better for higher loads.

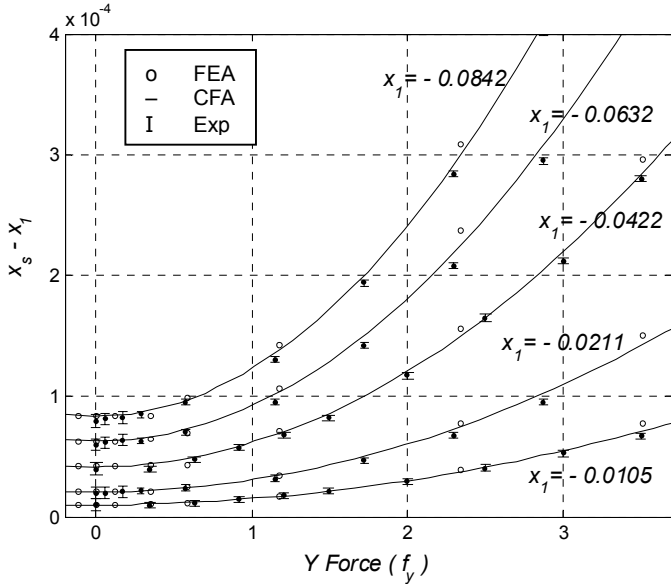


Fig. 11 Lost Motion and Inline Stiffness

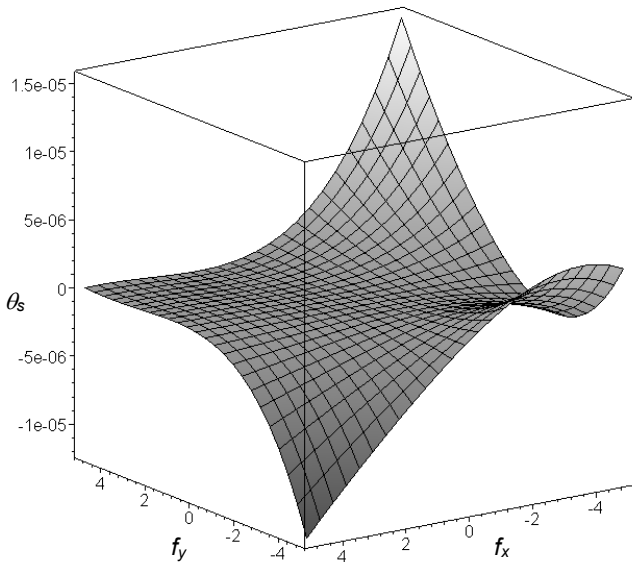


Fig.12 Motion Stage Rotation: CFA Prediction

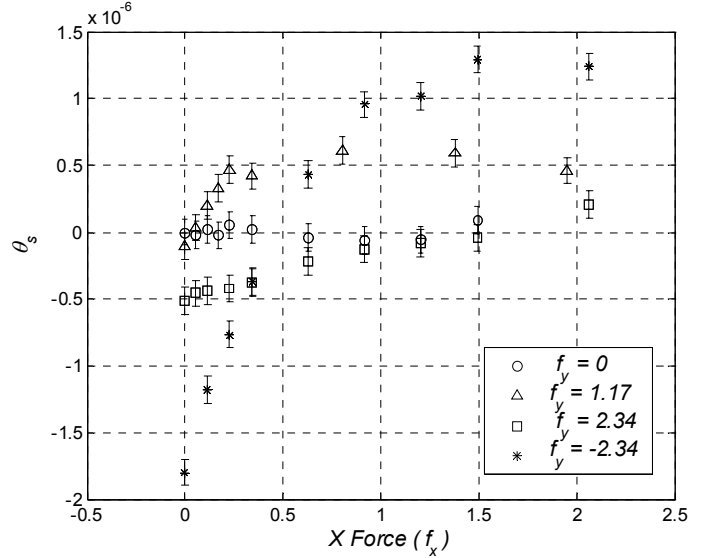


Fig.12 Motion Stage Rotation: Experimental Measurement

Finally, we present the rotation of the intermediate stages assuming general loads, but for specific cases to avoid complex expressions. For $f_y = 0 = m_y$,

$$\theta_1 = \left(\frac{64a^2 + rdf_x^2}{128a^2 + rdf_x^2} \right) \frac{[rdf_x^2 m_x - 32a^2 f_x (1 + 2a_o) + 320a^2 m_x]}{256a^2 \bar{w}^2 d}$$

$$\theta_2 = \left(\frac{64a^2 + rdf_x^2}{128a^2 + rdf_x^2} \right) \frac{[af_x (b_o - 0.5) - m_x a]}{4a\bar{w}^2 d}$$

$$\theta_7 = \left(\frac{64a^2 + rdf_x^2}{128a^2 + rdf_x^2} \right) \frac{[rdf_x^2 m_x + 32a^2 f_x (1 + 2a_o) + 64a^2 m_x]}{256a^2 \bar{w}^2 d}$$

$$\theta_8 = \left(\frac{64a^2 + rdf_x^2}{128a^2 + rdf_x^2} \right) \frac{[af_x (b_o - 0.5) + m_x a]}{4a\bar{w}^2 d}$$

These expressions provide the COS of the intermediate stage with respect to X actuation. Similarly, the intermediate stage rotations for a different loading condition are as follows. For $f_x = 0 = m_x$,

For $f_x = 0 = m_x$,

$$\theta_1 = \left(\frac{64a^2 + rdf_y^2}{128a^2 + rdf_y^2} \right) \frac{[af_y (b_o - 0.5) + m_y a]}{4a\bar{w}^2 d}$$

$$\theta_2 = \left(\frac{64a^2 + rdf_y^2}{128a^2 + rdf_y^2} \right) \frac{[rdf_y^2 m_y - 32a^2 f_y (1 + 2a_o) + 320a^2 m_y]}{256a^2 \bar{w}^2 d}$$

$$\theta_7 = \left(\frac{64a^2 + rdf_y^2}{128a^2 + rdf_y^2} \right) \frac{[af_y (b_o - 0.5) - m_y a]}{4a\bar{w}^2 d}$$

$$\theta_8 = \left(\frac{64a^2 + rdf_y^2}{128a^2 + rdf_y^2} \right) \frac{[rdf_y^2 m_y + 32a^2 f_y (1 + 2a_o) + 64a^2 m_y]}{256a^2 \bar{w}^2 d}$$

Assuming the forces are applied along the COS axes of the motion stage, rotations of the intermediate stages may be obtained by setting $m_x = m_y = 0$ in the above expressions. For the

given choice of $b_o=1/2$, it is seen that Stage 1 and Stage 3 rotations can be made insensitive to f_y , and Stage 2 and Stage 7 rotations can be made insensitive to f_x . In general, the intermediate stage rotations in this case are similar to the previous design, for a given overall range of motion.

FEA AND EXPERIMENTS

Plane-Strain based Finite Element Analysis was performed for both designs to validate the closed-form predictions. Dimensions used for Design 1 are $a_o=0.9737$, $b_o=0.5$, $t=1/76$, and $L=60mm$, and those for Design 2 are $a_o=0.9737$, $b_o=0.5$, $r_o=0.9737$, $t=1/76$, and $L=60mm$. The agreement between FEA and closed-form analysis (CFA) predictions is found to be within 8% in terms of numerical values and almost exact in terms of the non-linear trends, as evident from the plots. Primary motion stiffness predicted by FEA is found to be slightly lower as compared to CFA. The normalized axial stiffness, d , was found to be approximately 20% less than the theoretical value. This is corroborated by the experimental measurements, and is due to the compliance of the secondary stage of the double parallelogram modules [21], which is not accounted for in the CFA.

For the purpose of experimental verification, an AL6061-T6 prototype of XY Mechanism Design 2, was precisely fabricated using wire-EDM. The experimental set-up was designed such that the stage can be actuated using free weights, motorized precision micrometers, and piezoelectric stacks. The metrology consisted of plane-mirror laser interferometry, autocollimation and capacitance gages, to measure the translations and rotations of the motion and intermediate stages. Measurements were conducted on an isolation table, and corrected for temperature and humidity variations. Simultaneous measurements using multiple sensors and successive measurements using different actuators yield a reliable validation of the predicted properties of the XY mechanism, accurate to within 10%. Measurement uncertainty is approximately 50nm for displacements and 0.2 μ rad for rotations. The experiments reveal a slightly higher primary motion stiffness as compared to CFA prediction, likely due to an assumed value of Young's modulus.

CONCLUSION

This paper has presented two parallel kinematic XY flexure mechanism designs based on a constraint arrangement that allows large primary motions and small error motions. Key performance attributes and tradeoffs for XY mechanisms are have been explained. Closed-form nonlinear force-displacement model of the double parallelogram has been used quantify these performance attributes and tradeoffs. This nonlinear analysis reveals important elastokinematic effects that are not captured by linear analysis, which is thereby shown to be inadequate for performance evaluation over a large motion range. The need to minimize lost motion, motion stage rotation and cross-axis coupling, and to maintain inline stiffness and actuator isolation, conflicts with the desire for large range of motion. These

compromises depend on the characteristics of the building block modules and the geometry of the layout. It is shown that Design 2, owing to its higher degree of symmetry, exhibits lower cross-axis coupling and motion stage rotation in comparison to Design 1. However, other performance attributes such as lost motion, actuator isolation and inline stiffness, remain similar in nature and magnitude between the two designs. Furthermore, the concept of Center of Stiffness is discussed as an inexpensive means for the passive minimization of stage rotations. The effectiveness of this method is shown to be influenced by the mechanism's geometry, with the symmetric design proving to be a more suitable candidate.

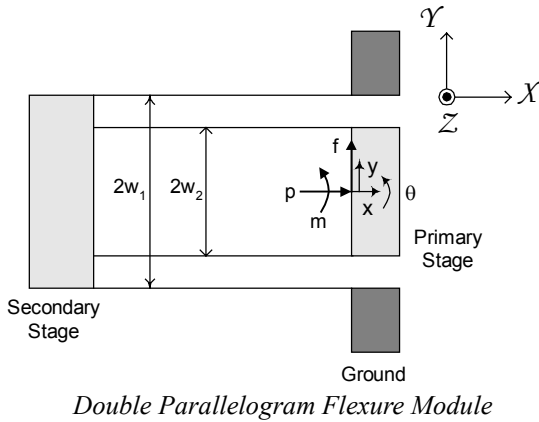
For motion stages designed for high dynamic performance, the inline elastokinematic stiffness can be considerably improved by the use of the double tilted-beam flexure module [20-21], which preserves axial stiffness but is detrimental to stage rotations. Dynamic, thermal and sensitivity analyses of the presented and similar designs are currently being pursued. In addition, an improved version of Design 2 is being developed for a high precision microscope positioning stage and a meso-scale machining center.

REFERENCES

1. Ryu, J.W., Gweon, D.-G., and Moon, K.S., 1997, "Optimal Design of a Flexure Hinge based X-Y- θ Wafer Stage", *Journal of Precision Engineering*, **21**(1), pp. 18-28.
2. Smith, A.R., Gwo, S., and Shih, C.K. 1994, "A New High Resolution Two-dimensional Micropositioning Device for Scanning Probe Microscopy", *Review of Scientific Instruments*, **64** (10), pp. 3216-3219.
3. Eom, T.B. and Kim, J.Y., 2001, "Long Range Stage for the Metrological Atomic Force Microscope", *Proc. of ASPE 2001 Annual Meeting*, pp. 156-159.
4. Gorman, J. J. and Dagalakis, N. G., 2003, "Force control of linear motor stages for microassembly", IMECE2003 – 42079, *ASME International Mechanical Engineering Conference and Exposition*, Washington, DC.
5. Vettiger, P., et al., 2000, "The Millipede – More than one thousand tips for future AFM data storage", *IBM Journal of Research and Development*, **44** (3), pp. 323-340.
6. ADXL Accelerometers and ADXRS Gyroscopes, www.analogdevices.com
7. Agilent Nanostepper J7220, www.labs.agilent.com
8. XY Nanopositioner P-733, www.physikinstrumente.com
9. Chang, S.H., Tseng, C.K., and Chien, H.C., 1999, "An Ultra-Precision XY θ_z Piezo-Micropositioner Part I: Design and Analysis", *IEEE Transactions on Ultrasonics, Ferroelectrics, and Frequency Control*, **46** (4), pp. 897-905.
10. Chen, K.S., Trumper, D.L., and Smith, S.T., 2002, "Design and Control for an Electromagnetically driven X-Y- θ Stage", *Journal of Precision Engineering and Nanotechnology*, **26**, pp. 355-369.

11. Awtar, S., 2004, "Analysis and Synthesis of Planer Kinematic XY Mechanisms", Sc.D. thesis, Massachusetts Institute of Technology, Cambridge, MA.
http://web.mit.edu/shorya/www
12. Ananthasuresh, G.K., Kota S., and Gianchandani, Y., 1994, "A Methodical Approach to Design of Compliant Micromechanisms", *Solid State Sensor and Actuator Workshop*, Hilton Head Island, SC, pp. 189-192.
13. Frecker, M.I., Ananthasuresh, G.K., Nishiwaki, S., Kickuchi, N., and Kota S., 1997, "Topological Synthesis of Compliant Mechanisms Using Multi-criteria optimization," *Journal of Mechanical Design*, **119**, pp. 238-245.
14. Blanding, D.K., 1999, *Exact Constraint: Machine Design Using Kinematic Principles*, ASME Press, New York, NY.
15. Awtar S., and Slocum A.H., 2004, "Apparatus Having motion with Pre-determined degree of Freedom", US Patent 6,688,183 B2.
16. Bisshopp, K.E., and Drucker, D.C., 1945, "Large Deflection of Cantilever Beams", *Quarterly of Applied Mathematics*, **3** (3), pp. 272-275.
17. Howell L.L., 2001, *Compliant Mechanisms*, John Wiley & Sons, New York, NY.
18. Plainevaux, J.E., 1956, "Etude des deformations d'une lame de suspension elastique", *Nuovo Cimento*, **4**, pp. 922-928.
19. Legtenberg, R., Groeneveld, A.W. and Elwenspoek, M., 1996, "Comb-drive Actuators for Large Displacements", *Journal of Micromechanics and Microengineering*, **6**, pp. 320-329.
20. Awtar S., and Slocum A.H., 2005, "Closed-form Nonlinear Analysis of Beam-based Flexure Modules", DETC2005-85440, *Proc. ASME IDETC/CIE 2005*, Long Beach, CA.
21. Saggere, L., Kota, S., 1994, "A New Design for Suspension of Linear Microactuators", *ASME Journal of Dynamic Systems and Control*, **55** (2), pp. 671-675.

APPENDIX [11, 20]



Normalized transverse force, moment, axial force, transverse displacement, rotation, and axial displacement at the double parallelogram primary stage are denoted by f , m , p , y , θ , and x , respectively. $a=12$, $c=-6$, $e=1.2$, $i=-0.6$, $h = -0.1$, and r

$=1/700$ are dimensionless numbers characteristic of the uniform cross-section beam. $d = 12(1-\nu^2)/t^2$ is the normalized axial beam stiffness, where ν is Poisson's ratio and t the normalized beam thickness. The sub-script λ in the following expressions denotes a given double parallelogram flexure module's reference number.

Linear Analysis

$$\begin{bmatrix} x_\lambda \\ y_\lambda \\ \theta_\lambda \end{bmatrix} = \begin{bmatrix} \frac{1}{d} & 0 & 0 \\ 0 & \frac{1}{a} & \frac{1}{2\bar{w}^2 d} \\ 0 & \frac{1}{2\bar{w}^2 d} & \frac{1}{\bar{w}^2 d} \end{bmatrix} \begin{bmatrix} p_\lambda \\ f_\lambda \\ m_\lambda \end{bmatrix} \quad \text{where} \quad \bar{w}^2 \triangleq \frac{2w_1^2 w_2^2}{w_1^2 + w_2^2}$$

Nonlinear Analysis

$$y_\lambda \approx \frac{4af_\lambda}{(2a)^2 - (ep_\lambda)^2}$$

$$x_\lambda = \frac{p_\lambda}{d} + p_\lambda y_\lambda^2 \frac{r[(2a)^2 + (ep_\lambda)^2] - 8aei}{(4a)^2}$$

$$\theta = [fn_1(p_\lambda) \quad fn_2(p_\lambda) \quad fn_3(p_\lambda) \quad fn_4(p_\lambda)] \begin{bmatrix} f_\lambda \\ m_\lambda \\ f_\lambda^3 \\ m_\lambda f_\lambda^2 \end{bmatrix}$$

where,

$$fn_1(p_\lambda) = \frac{[1 \quad p_\lambda \quad p_\lambda^2] \begin{bmatrix} 4a^2 w_2^2 + 4ac(w_2^2 - w_1^2) \\ -2ah(w_2^2 + w_1^2) + 2ce(w_2^2 + w_1^2) - 2aw_2^2 \\ he(w_1^2 - w_2^2) + w_2^2 e(1-e) \end{bmatrix}}{2dw_1^2 w_2^2 ((2a)^2 - (ep_\lambda)^2)}$$

$$fn_2(p_\lambda) = \frac{(w_2^2 + w_1^2)}{2dw_1^2 w_2^2}$$

$$fn_3(p_\lambda) = \frac{r[1 \quad p_\lambda \quad p_\lambda^2 \quad p_\lambda^3 \quad p_\lambda^4]}{2w_1^2 w_2^2 ((2a)^2 - (ep_\lambda)^2)^3}$$

$$\begin{bmatrix} 16a^4 w_2^2 + 16a^3 c(w_2^2 - w_1^2) \\ -8a^3 h(w_2^2 + w_1^2) + 24a^2 ce(w_2^2 + w_1^2) - 8a^3 w_2^2(1-2e) \\ 12ace^2(w_2^2 - w_1^2) + 12a^2 he(w_1^2 - w_2^2) - 4a^2 w_2^2 e \\ -6ahe^2(w_2^2 + w_1^2) + 2ce^3(w_2^2 + w_1^2) + 2aw_2^2 e^2(1-2e) \\ he^3(w_1^2 - w_2^2) + w_2^2 e^3(1-e) \end{bmatrix}$$

$$fn_4(p_\lambda) = \frac{r[1 \quad p_\lambda \quad p_\lambda^2] \begin{bmatrix} 4a^2(w_2^2 + w_1^2) \\ 4ae(w_2^2 - w_1^2) \\ e^2(w_2^2 + w_1^2) \end{bmatrix}}{2w_1^2 w_2^2 ((2a)^2 - (ep_\lambda)^2)^2}$$